Accepted Manuscript

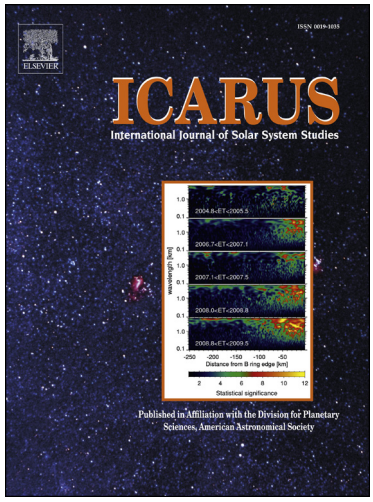

Characterization of Artifacts Introduced by the Empirical Volcano-Scan Atmospheric Correction Commonly Applied to CRISM and OMEGA Near-Infrared Spectra

S.M. Wiseman, R.E. Arvidson, M.J. Wolff, M.D. Smith, F.P. Seelos, F. Morgan, S.L. Murchie, J.F. Mustard, R.V. Morris, D. Humm, P.C. McGuire

PII: S0019-1035(14)00551-X
DOI: http://dx.doi.org/10.1016/j.icarus.2014.10.012
Reference: YICAR 11312

To appear in: *Icarus*

Received Date: 3 May 2013
Revised Date: 3 October 2014
Accepted Date: 7 October 2014

Please cite this article as: Wiseman, S.M., Arvidson, R.E., Wolff, M.J., Smith, M.D., Seelos, F.P., Morgan, F., Murchie, S.L., Mustard, J.F., Morris, R.V., Humm, D., McGuire, P.C., Characterization of Artifacts Introduced by the Empirical Volcano-Scan Atmospheric Correction Commonly Applied to CRISM and OMEGA Near-Infrared Spectra, *Icarus* (2014), doi: http://dx.doi.org/10.1016/j.icarus.2014.10.012

Characterization of Artifacts Introduced by the Empirical Volcano-Scan Atmospheric Correction Commonly Applied to CRISM and OMEGA Near-Infrared Spectra

S. M. Wiseman[1], R. E. Arvidson[2], M. J. Wolff[3], M. D. Smith[4], F. P. Seelos[5], F. Morgan[5], S. L. Murchie[5], J. F. Mustard[1], R. V. Morris[6], D. Humm[7], P. C. McGuire[8,5]

[1]Department of Earth, Environmental and Planetary Sciences, Brown University, Providence, RI, USA.

[2]McDonnell Center for the Space Sciences, Department of Earth and Planetary Sciences, Washington University in Saint Louis, Saint Louis, Missouri, USA.

[3]Space Science Institute, Boulder, Colorado, USA.

[4]NASA Goddard Space Flight Center, Greenbelt, Maryland, USA.

[5]Johns Hopkins University Applied Physics Laboratory, Laurel, Maryland, USA.

[6]NASA Johnson Space Center, Houston, Texas, USA.

[7]Space Instrument Calibration Consulting, Annapolis, MD, USA.

[8]Planetary Sciences and Remote Sensing Group, Institute of Geological Sciences, Freie Universitaet Berlin, Berlin, Germany.

Corresponding Author Contact Information:
Sandra M. Wiseman
Department of Earth, Environmental and Planetary Sciences
Brown University
324 Brook St., Box 1846
Providence, RI 02912, USA
Telephone: (401) 863-9663
Fax: (401) 863-3978
Email: sandra_wiseman@brown.edu

Icarus #11312

Characterization of Artifacts Introduced by the Empirical Volcano-Scan Atmospheric Correction Commonly Applied to CRISM and OMEGA Near Infrared Spectra

S. M. Wiseman, R. E. Arvidson, M. J. Wolff, M. D. Smith, F. P. Seelos, F. Morgan, R. V. Morris, J. F. Mustard, D. Humm, S. L. Murchie, P. C. McGuire

Abstract

The empirical 'volcano-scan' atmospheric correction is widely applied to Martian near infrared CRISM and OMEGA spectra between ~1000 and ~2600 nm to remove prominent atmospheric gas absorptions with minimal computational investment. This correction method employs division by a scaled empirically-derived atmospheric transmission spectrum that is generated from observations of the Martian surface in which different path lengths through the atmosphere were measured and transmission calculated using the Beer-Lambert Law. Identifying and characterizing both artifacts and residual atmospheric features left by the volcano-scan correction is important for robust interpretation of CRISM and OMEGA volcano-scan corrected spectra. In order to identify and determine the cause of spectral artifacts introduced by the volcano-scan correction, we simulated this correction using a multiple scattering radiative transfer algorithm (DISORT). Simulated transmission spectra that are similar to actual CRISM- and OMEGA-derived transmission spectra were generated from modeled Olympus Mons base and summit spectra. Results from the simulations were used to investigate the validity of assumptions inherent in the volcano-scan correction and to identify artifacts introduced by this method of atmospheric correction. We found that the most prominent artifact, a bowl-shaped feature centered near 2000 nm, is caused by the inaccurate assumption that absorption coefficients of CO_2 in the Martian atmosphere are independent of column density. In addition, spectral albedo and slope are modified by atmospheric aerosols. Residual atmospheric contributions that are caused by variable amounts of dust aerosols, ice aerosols, and

water vapor are characterized by the analysis of CRISM volcano-scan corrected spectra from the same location acquired at different times under variable atmospheric conditions.

1 Introduction

Images of the Martian surface acquired by the NASA Mars Reconnaissance Orbiter (MRO) Compact Reconnaissance Imaging Spectrometer for Mars (CRISM) [*Murchie et al.*, 2007] and the Mars Express Observatoire pour la Minéralogie, l'Eau, les Glaces et l'Activité (OMEGA) [*Bibring et al*., 2004; 2005] measure solar light that was attenuated and scattered as it traversed down through the Martian atmosphere, interacted with the surface, and traversed up through the atmosphere. Therefore, each spectrum from standard CRISM and OMEGA observations contains contributions from atmospheric gases (e.g., CO_2, CO, and H_2O), atmospheric aerosols (e.g., dust and water ice), and the surface. Atmospheric gas contributions dominate the spectrum at wavelengths that CO_2 absorbs (Figure 1).

The empirical 'volcano-scan' correction [*Bibring et al*., 1989; *Langevin et al*., 2005; *McGuire et al.*, 2009] is widely applied to CRISM and OMEGA near infrared (NIR) spectra between ~1000 and ~2600 nm to remove prominent atmospheric gas absorptions with minimal computational investment. The volcano-scan correction method employs division by a scaled atmospheric transmission spectrum that is generated from observations of the Martian surface in which different path lengths through the atmosphere were measured. Low and high altitude spectra acquired over the base and summit of the Olympus Mons volcano were used, giving the correction its name. Transmission is calculated empirically using the Beer-Lambert Law, as detailed in section 2.2.

Although the volcano-scan correction removes prominent gas absorptions to first order, closer inspection reveals that corrected spectra exhibit spurious features in areas of strong gas absorption. The most prominent artifact is a bowl-shaped feature that overlaps with the CO_2 triplet centered near 2000 nm (Figure 1). The volcano-scan correction can be applied automatically to CRISM images using publically available CRISM Analysis Tools (CAT) software released through the Planetary Data System (PDS). The current version of CAT at this time (version 7.2.1) includes an option to empirically correct the 2000 nm bowl-shaped artifact that is evident in volcano-scan corrected images on a pixel by pixel basis.

The occurrence of the apparent bowl-shaped artifact at 2000 nm could have several causes. There are three major assumptions implicit in deriving empirical transmission spectra: 1) surface contributions to the low and high altitude spectra used to create transmission spectra are equivalent and therefore cancel out, 2) aerosol contributions to low and high altitude spectra can be ignored both within and outside of gas absorption lines and therefore empirical transmission spectra contain molecular absorption only, 3) absorption coefficients of CO_2 in the Martian atmosphere are independent of column density and absorption strength therefore scales exponentially with column density.

In order to identify and determine the cause of artifacts introduced by the volcano-scan correction method, we simulated this correction using a multiple scattering radiative transfer algorithm. Discrete Ordinate Radiative Transfer (DISORT) modeling allows for the explicit treatment of aerosol, gas, and surface contributions simultaneously [*Stamnes et al.*, 1988; *Thomas and Stamnes*, 2002]. The DISORT radiative transfer model was used to calculate modeled high and low altitude spectra similar to Martian spectra of Olympus Mons. Simulated transmission spectra were derived from these modeled spectra using the same method that was

used to produce CRISM- and OMEGA-derived transmission spectra. Generating simulated transmission spectra in this manner and applying them to modeled Martian spectra using the volcano-scan correction method allows the variables related to the three major assumptions described above to be controlled and analyzed.

Because the volcano-scan correction is designed to remove absorptions from atmospheric CO_2, this correction does not specifically address contribution from other atmospheric species, including dust and ice aerosols and gaseous water vapor. CO absorption is minor (Figure 1, gray arrow) and will not be considered. Aerosol and water vapor atmospheric contributions are particularly important because they are spatially and temporally variable [e. g., *Smith et al*., 2008] and produce noticeable features in CRISM and OMEGA spectra [e. g., *Smith et al*., 2009]. Dust aerosol contributions affect spectral slope and amplitude and ice aerosols also have distinct absorption features in the NIR. In addition, aerosol scattering within gas absorption lines alters absorption features. Atmospheric water vapor absorptions that occur in empirically derived transmission spectra cannot be scaled separately from CO_2 absorptions in the transmission spectrum that is scaled during the volcano-scan correction. Failure to explicitly address atmospheric water vapor can cause under- and over-corrected water vapor features in volcano-scan corrected spectra.

Identifying and characterizing both artifacts and residual atmospheric features left by the volcano-scan correction is important for proper interpretation of CRISM and OMEGA volcano-scan corrected spectra. Results from the simulated volcano-scan correction are used to investigate the validity of assumptions inherent in deriving and applying empirical transmission spectra and to identify and determine the causes of artifacts (e.g., 2000 nm bowl-shape) introduced by this atmospheric correction method. In addition, we characterize spectral features

that result from dust aerosols, ice aerosols, and water vapor that are not specifically addressed by the volcano-scan correction. Variations in these species cause volcano-scan corrected spectra to exhibit variable residual features depending on atmospheric conditions at the time of image acquisition. These residual features and artifacts are highlighted by comparison of CRISM volcano-scan corrected spectra from the same location on Mars but acquired at different times under variable atmospheric conditions.

2 Background

2.1 CRISM and OMEGA Datasets

The CRISM spectrometer has short (S) and long (L) wavelength detectors that operate between 360 to 1053 nm and 1003 to 3920 nm, respectively [*Murchie et al*., 2007; 2009]. CRISM is capable of acquiring hyperspectral images with 544 channels spaced ~7 nm apart. CRISM is mounted on a gimbal platform that allows ground tracking of a target to acquire full resolution targeted (FRT) images with up to 20 m/pixel spatial resolution. The CRISM spectrometer utilizes 2-dimensional detector arrays that cause slight column dependencies in CRISM spectral data, including a smooth variation in the central wavelength position of each channel [*Murchie et al*., 2007]. Image rows are built up as a result of along track spacecraft motion. CRISM I/F (where I is the radiance at sensor divided by the solar irradiance, F, at the top of the Martian atmosphere divided by π) spectra available from the PDS (http://pds-geoscience.wustl.edu) were calibrated as described by *Murchie et al.* [2007, 2009].

Atmospheric transmission files derived from CRISM hyperspectral, non-gimbaled FFC images acquired at the base and summit of Olympus Mons are contained in Atmospheric Transmission (AT) Calibration Data Record (CDR) files that are available through the PDS.

Because a relatively small (< 1.5 nm) temperature dependent wavelength shift is observed in CRISM L detector spectra [*Smith et al.,* 2009], AT CDRs for several different wavelength shifts were derived. A slope correction was applied to transmission spectra in the AT CDR files in an effort to normalize the shapes of the transmission spectra and ensure that continuum values are near unity. The most current version of CAT at this time (version 7.2.1) includes an option to empirically correct the 2000 nm bowl-shaped artifact that is evident in volcano-scan corrected images on a pixel by pixel basis (algorithm developed by Frank Morgan and formulation present in CAT v7.2.1 code). The 2000 nm bowl-shaped artifact is defined relative to a straight line continuum derived from a reference observation. The same low altitude Olympus Mons spectra used to generate empirical transmission spectra are used to define the artifact (to minimize temperature dependent wavelength shift and surface variations) for wavelengths between ~1760 and 2240 nm. The artifact correction spectrum is determined by subtracting the volcano-scan corrected reference spectrum from the continuum fit to that spectrum. After the volcano-scan correction is applied, the artifact correction spectrum is multiplicatively scaled to match the artifact expressed in each pixel. The 2000 nm bowl-shaped artifact is then corrected by adding the scaled artifact correction to the volcano-scan corrected spectrum, for each pixel in the image.

The OMEGA spectrometer [*Bibring et al.,* 2004] covers the wavelength range from 350 to 5100 nm in 352 channels using VNIR (350 to 1070 nm), C (930 to 2700 nm), and L (2530 to 5100 nm) detectors. C detector channels have a wavelength spacing of ~14 nm [*Bibring et al.* 2004, 2005]. Images vary in spatial resolution depending on spacecraft altitude and are built up by across track scanning and along track spacecraft motion. OMEGA data lack the column dependent issues inherent in CRISM data. OMEGA images as well as software to calibrate and process the images to units of I/F as described by *Bibring et al.* [2004, 2005], are available

through the PDS at http://pds-geoscience.wustl.edu. An OMEGA-derived atmospheric transmission spectrum for use with the empirical volcano-scan correction is not publically available but can be calculated from Olympus Mons observations using methods described in the following section.

2.2 Empirical Volcano-Scan Correction

The empirical volcano-scan correction method relies on empirically derived transmission spectra to remove CO_2 absorption features from spectra of the Martian surface [*Bibring et al.*, 1989; *Langevin et al.*, 2005; *McGuire et al.*, 2009]. Transmission spectra are generated from observations in which different path lengths through the atmosphere were measured. High altitude spectra were acquired at the summit of Olympus Mons (~20 km above datum) and low altitude spectra at its base (~0 km) (Figure 2a). Transmittance between the base and summit of Olympus Mons is determined using the Beer-Lambert Law (equation 1) integrated with the assumption that the absorption coefficient, *k*, is constant with height in the atmosphere (equation 2).

$$T(\lambda) = I_\lambda(s_{0\to 2}) / I_\lambda(s_{0\to 1}) = e^{-\int_{s1}^{s2} k\,ds} \quad (1)$$

$$T(\lambda) = I_\lambda(s_{0\to 2}) / I_\lambda(s_{0\to 1}) = e^{-k s_{1\to 2}} = e^{-\tau} \quad (2)$$

$$-ln\left(T(\lambda)\right) = k s_{1\to 2} = \tau \quad (3)$$

In equations 1 through 3, T is transmittance, I_λ is equivalent to CRISM or OMEGA I/F at wavelength (λ), $s_{0\to 1}$ is the sum of the incoming and outgoing path lengths from the top of the atmosphere (s_0) to height s_1 within the atmosphere, $s_{0\to 2}$ is the sum of the incoming and outgoing

path lengths from the top of the atmosphere (s_0) to height s_2 within the atmosphere, and τ is the total extinction. Note, for nonzero solar incidence (*i*) angles or detector emission (*e*) angles, the incoming path length is equal to the height (s_0 or s_1) divided by cos(*i*) and the outgoing path length is the height divided by cos(*e*). Implicit in equation (2) is that the surface contribution to $I_\lambda(s_{0\rightarrow1})$ and $I_\lambda(s_{0\rightarrow2})$ is identical and that *k* is independent of path length (*s*). The effects of aerosol scattering within wavelengths of gas absorption are ignored for the purposes of deriving empirical transmission spectra and τ is assumed to result from molecular absorption only. Although *T* at wavelengths outside of gas bands should equal unity, in practice, the ratio of the low and high altitude spectra must be multiplicatively scaled to ~1.0 at wavelengths outside of gas absorptions to account for differences in surface spectral features and/or aerosol opacities in high and low altitude spectra.

To perform the volcano-scan correction for an arbitrary CRISM or OMEGA I/F spectrum, the empirically derived transmission spectrum is scaled using an exponential factor determined so that the most prominent CO_2 absorption feature in the transmission spectrum has an equivalent depth to the same CO_2 feature in the I/F spectrum that is to be corrected, as described below. For simplicity, the 'I/F spectrum that is to be corrected' will be referred to as the target I/F spectrum. That is, division of the surface spectrum by the scaled transmission spectrum, in principle, eliminates CO_2 absorption features from the target I/F spectrum. During application of the volcano-scan correction, the transmission spectrum must be scaled separately for each target I/F spectrum because the surface pressure, which affects the depth of CO_2 absorptions, varies as a function of surface elevation and solar longitude (L_s) (e. g., *Smith et al.*, 2004). Calculating the exponential scaling factor that is needed for the most prominent CO_2 feature in the transmission spectrum to match up with the depth of the same CO_2 feature in the

target I/F spectrum relies on band depth estimates. The band depth of an absorption feature in the target I/F spectrum and the band depth of the same feature in the empirical transmission spectrum are proxies for the transmittance that occurred over the atmospheric path lengths traversed for the I/F target spectrum and the empirical transmission spectrum, respectively. In the equations below, the arbitrary CRISM or OMEGA I/F spectrum that is to be corrected is labeled 'target', the transmission spectrum is labeled 'trans', $I_{feature}$ is the I/F value of a CO_2 absorption feature at some wavelength, $T_{feature}$ is the transmission value of a CO_2 absorption feature at the same wavelength, and BD is the band depth of that CO_2 feature. The target I/F spectrum has an arbitrary atmospheric path length of $s_{0\rightarrow 3}$.

$$BD_{targ} = I_{feature}\left(target\right)/I_{continuum}\left(target\right), \tag{4}$$

assuming $T = 1$ on the continuum,

$$BD_{targ} = I_{feature}\left(s_{0\rightarrow 3}\right)/I_{continuum} = \mathrm{e}^{-\mathrm{k}s_{0\rightarrow 3}}, \tag{5}$$

Similarly,

$$BD_{trans} = T_{feature}\left(trans\right)/T_{continnum}\left(trans\right), \tag{6}$$

$$BD_{trans} = T_{feature}\left(s_{1\rightarrow 2}\right)/T_{continnum} = e^{-k_{s1\rightarrow s2}}. \tag{7}$$

The exponential scaling factor is determined from

$$\ln\left(BD_{targ}\right)/\ln\left(BD_{trans}\right) = \ln\left(e^{-ks_{0\rightarrow 3}}\right)/\ln\left(\mathrm{e}^{-\mathrm{k}s_{1\rightarrow 2}}\right) = s_{0\rightarrow 3}/s_{1\rightarrow 2}. \tag{8}$$

Because the exponential scaling factor represents the difference in path length between the target spectrum and the transmission spectrum, its value should be the same for all

wavelengths. However, uncertainties are associated with determining the band depth from CRISM spectra. An estimate of the band depth for the strongest CO_2 band in the CO_2 triplet near 2000 nm is commonly calculated as the ratio of the slope corrected I/F value along the continuum at ~1900 nm to the I/F value in the CO_2 absorption feature at ~2010 nm. OMEGA measures only a single channel near 2010 nm, which is located at 2012 nm, whereas CRISM has channels at 2007 and 2014 nm. *McGuire et al.*, [2009] note that variations in the surface spectral contribution between the wavelength along the continuum and the wavelength of the CO_2 absorption feature can cause error in the calculated band depth and instead suggests using the ratio of the I/F continuum value at 1980 nm to the I/F value of the CO_2 absorption feature at 2007 nm. These two band depth estimates will be referred to as the BD1 and BD2, respectively. All wavelengths of the transmission spectrum are scaled by the single (wavelength independent) exponential factor calculated using the band depth estimate.

Applying the volcano-scan correction to the target spectrum of interest, remembering that

$$I_\lambda\left(s_{0\to 3}\right) = I_\lambda\left(s_0\right) * e^{-ks_{0\to 3}}, \tag{9}$$

results in

$$I_{feature}\left(s_0\right) e^{-ks_{0\to 3}} \Big/ \left(e^{-ks_{1\to 2}}\right)^{s_{0\to 3}/s_{1\to 2}} = I_{feature}\left(s_0\right), \tag{10}$$

where $I_{feature}\left(s_0\right)$ is the CRISM or OMEGA I/F value corrected for gas absorption, provided that all assumptions inherent in the volcano-scan correction are valid.

2.3 Radiative Transfer Modeling

Our radiative transfer modeling utilized a publically available general purpose Fortran program for discrete-ordinate-method radiative transfer in scattering and emitting layered media, Discrete Ordinate Radiative Transfer (DISORT) [*Stamnes et al*., 1988; *Thomas and Stamnes*, 2002]. The atmosphere is treated as a plane-parallel medium in which individual layers are homogenous but interlayer properties can be varied. Attenuation and scattering of the solar beam down through the atmosphere, interaction with the surface, and attenuation and scattering up through the atmosphere are modeled. The numerical implementation is discussed in *Stamnes et al*., [1999] and *Thomas and Stamnes* [2002]. Gas absorptions from CO_2, CO, and H_2O were defined using correlated-k distributions with parameters derived from the HITRAN database [*Rothman et al.,* 2005].

We utilized 'front-end' routines optimized for study of the Martian atmosphere, DISORT_multi, to compute modeled CRISM and OMEGA I/F spectra [*Wolff et al*., 2009]. Atmospheric temperature profiles relevant to atmospheric conditions at the latitude, longitude, and Ls of interest were derived from spatially binned Mars Global Surveyor Thermal Emission Spectrometer (TES) observations of Mars acquired between 1998 and 2000 [*Smith*, 2004]. Dust aerosol single scattering albedos for 1.5 μm particles and wavelength dependent phase functions utilized in our modeling were derived from analysis of CRISM hyperspectral data [*Wolff et al.*, 2009]. DISORT modeled I/F spectra presented in this paper are similar to those that would be observed at the top of the Martian atmosphere by CRISM or OMEGA. Similar procedures were described by *Arvidson et al*. [2006]. Absorption, emission, and multiple scattering from atmospheric gases and aerosols were modeled.

3. Volcano-Scan Correction Simulation Results

To evaluate the validity of assumptions implicit in deriving empirical transmission spectra and to identify and determine causes of artifacts introduced by application of the volcano-scan correction, we simulated the volcano-scan correction using DISORT radiative transfer modeling. Comparing volcano-scan corrected spectra generated using simulated transmission spectra applied to modeled surface spectra enables identification and characterization of artifacts introduced by the volcano-scan correction without the ambiguity inherent in real data because all variables can be controlled and systematically varied. In this section, we assessed potential artifacts that could arise from variation in surface spectral features and atmospheric dust aerosols present in high and low altitude spectra used to generate empirical transmission spectra as well as from ranges of exponential scaling factors potentially used during application of the volcano-scan correction.

3.1 Simulation of CRISM and OMEGA Empirical Transmission Spectra

In order to demonstrate that simulated transmission spectra are similar to actual CRISM- and OMEGA-derived transmission spectra, our initial simulation results were aimed at approximating measured high and low altitude Olympus Mons spectra. Although we modeled empirical transmission spectra that appear similar to both CRISM and OMEGA empirical transmission spectra (Figure 3), we focus on CRISM results. The higher spectral resolution of CRISM data (Figure 1) allows for more detailed characterization of artifacts. In addition, the volcano-scan correction as applied to CRISM spectra has the added complication of a temperature dependent wavelength shift, which we explore.

We chose to model CRISM high and low altitude spectra of Olympus Mons from FFC000061C4. Figure 2a shows that the high and low altitude CRISM spectra do not overlap

and that the summit spectrum is slightly darker than the base spectrum. The dust aerosol contribution is expected to be much less at the summit than at the base of Olympus Mons because, in a uniformly mixed atmosphere, the amount of aerosol particles is proportional to the atmospheric column density, which is much less at 20 km than 0 km altitude. Given the expected small dust aerosol contribution at the summit of Olympus Mons, we attempted to reproduce the low and high altitude spectra by modeling equivalent surface spectral properties in the high and low altitude spectra, modest dust opacity for the low altitude spectrum, and zero dust opacity for the summit spectrum. The surface spectrum was modeled as a straight line with a positive slope. It was necessary to lower the surface albedo of the high altitude spectrum by 5% relative to the low altitude spectrum (shown in Figure 4b) to produce modeled base and summit I/F spectra that are similar to measured base and summit I/F spectra (Figure 3). The simulated transmission spectrum has values near 1.1 on the continuum (Figure 3b, gray line) rather than expected values of 1.0, similar to the CRISM-derived transmission spectrum (Figure 2b, gray). Therefore, it was multiplicatively scaled to equal unity at wavelengths lacking gas absorption (Figure 3b, black line) as was done for the actual CRISM-derived transmission spectrum (Figure 2b, black line).

We produced simulated transmission spectra that appear broadly similar to actual CRISM- and OMEGA-derived transmission spectra (Figure 3c, d). Volcano-scan corrections using the simulated transmission spectra shown in Figure 3 were applied to modeled low altitude Olympus Mons spectra in order to demonstrate that our simulated volcano-scan correction results are similar to CRISM and OMEGA volcano-scan corrected spectra (Figure 4). Gaussian noise with a standard deviation of 1% was added to the modeled I/F spectrum prior to application of the volcano-scan correction to make the results more realistic. The resulting simulated volcano-

scan corrected spectra shown in Figure 4 are similar to actual CRISM and OMEGA volcano-scan corrected spectra shown in Figure 1. The bowl-shape evident at 2000 nm (Figure 4) is similar to the bowl-shaped artifact observed in CRISM and OMEGA volcano-scan corrected spectra (Figure 1) even though the modeled input spectrum was linear (Figure 4b, c gray line). This indicates that our simulation results are sufficient to characterize artifacts introduced by the volcano-scan correction.

3. 2 Impact of Aerosols and Surface Contributions in Transmission Spectra on the 2000 nm Bowl-Shaped Artifact

Two assumptions in empirically derived transmission spectra are that surface contributions to low and high altitude spectra used to create transmission spectra are equivalent and aerosol contributions to low and high altitude spectra can be ignored. If these assumptions are valid, then spectral contributions should be equivalent outside wavelengths of gas absorption in the low and high altitude spectra, and the base and summit spectra should overlap at these wavelengths, resulting in empirical transmission spectra having values of unity outside of gas absorptions. This is not the case (Figure 2a) and CRISM empirical transmission spectra must be multiplicatively scaled so that continuum values are near unity (Figure 2b). The transmission spectrum simulation results shown in Figure 4, in which the 2000 nm bowl-shaped artifact is evident, were generated to appear similar to CRISM and OMEGA data and had variable surface albedos (but no absorption feature at 2000 nm) and aerosol opacities between base and summit spectra.

In order to determine whether or not surface spectral features and atmospheric dust aerosols present in the high and low altitude spectra used to generate empirical transmission

spectra are responsible for the 2000 nm bowl-shaped artifact in the corrected spectra, we show simulation results in which these two variables are equivalent in the low and high altitude spectra. Figure 5a shows simulation results in which the base and summit spectra were identical (assumption 1 satisfied) and aerosol opacities were identical. The 2000 nm bowl-shaped artifact is evident. Figure 5b shows a similar simulation in which no aerosols were modeled (both assumption 1 and 2 satisfied). This simulation demonstrates that a 2000 nm bowl-shaped artifact occurs independently of the presence of aerosols and surface variability in the high and low altitude spectra used to generate empirical transmission spectra. Although a surface absorption feature near 2000 nm present in the base or summit spectrum could contribute to a 2000 nm artifact, such a feature is not required to explain the observed 2000 nm bowl-shaped artifact in CRISM volcano-scan corrected spectra (Figure 1). However, it is important to note that variable aerosol contributions between the empirical transmission spectrum and the spectrum to be corrected causes a mismatch in shape between gas bands that results from aerosol scattering into gas lines. This mismatch in shape between gas bands in the transmission spectrum and the spectrum to be corrected causes additional artifacts near 2000 nm (section 4).

3. 3 Impact of Exponential Scaling Factor on the 2000 nm Artifact

The gas absorption coefficient (k) is assumed to be constant (equation 2) in the calculation of the empirical transmission spectra. The volcano-scan correction is enabled by this assumption (equations 4-8). During the application of the volcano-scan correction, the empirical transmission spectrum is scaled exponentially by a single (wavelength independent) exponential scaling factor that is calculated so that the strength of its strong CO_2 absorption near 2010 nm is similar in strength to the same CO_2 feature in the spectrum to be corrected so that CO_2

absorptions can be divided out (see section 2.2). Small changes to the value of the exponential scaling factor alter the expressions of the artifacts observed near 2000 nm in volcano-scan corrected spectra (Figure 6). In the absence of artifacts, too small of an exponential scaling factor would result in a residual CO_2 triplet near 2000 nm and too large of a scaling factor would result in an inverse triplet. Applying the scaling factor calculated using the BD1 estimate results in 'hash' superimposed on the bowl-shaped artifact near 2000 nm caused by over correction of some parts of the CO_2 triplet, even though under correction of weaker CO_2 bands is evident at other wavelengths (Figure 6). Applying the scaling factor calculated using the BD2 estimate results in under correction of the CO_2 triplet near 2000 nm that has the appearance of a deeper bowl-shape (Figure 6). This is because the BD2 estimate results in a consistently smaller calculated exponential scaling factor. The addition of noise to the simulation (Figure 6b) reduces the structured appearance of the residual gas bands but does not mask them. Similar artifacts are evident in volcano-scan corrected CRISM spectra that were corrected using variable scaling factors (Figure 6c), and there does not appear to be a single exponential scaling factor that mitigates both the 'hash' and bowl-shape near 2000 nm (Figures 6).

The variable appearance of the artifact at 2000 nm in simulated and actual volcano-scan corrected spectra caused by using different exponential scaling factors to scale the transmission spectrum prior to its division demonstrates that assumption 3 is invalid and causes a prominent artifact at 2000 nm and smaller artifacts at other wavelengths of CO_2 absorption. Gas bands that appear broad at CRISM and OMEGA spectral resolution contain many individual absorption lines which have variable strengths (Figure 7a). Larger absorption coefficients and/or more molecules (higher column density) in the path length result in stronger and broader lines. A detailed discussion of gas line broadening and the curve of growth in the context of radiative

transfer modeling can be found in *Thomas and Stamnes*, [2002]. In the weak line limit ($\tau << 1$), or linear regime, wings of individual lines do not completely overlap and the absorptance (1 - *T*) is proportional to the amount of absorbing molecules. In the strong line limit ($\tau >> 1$), or saturated regime, there is a square root dependence on column density. In between these two limits, the wings of the gas lines overlap but the gas lines do not saturate, the absorption coefficient (*k*) is constant with column density, and an exponential relationship between absorptance and column density is observed. This regime is described by the integrated form of the Beer-Lambert Law in which *k* is assumed to be constant for each wavelength (equation 2). According to equation 3, -ln(*T*) should be linearly proportional to the path length, *s*, with the slope equal to *k*. A plot of *T* calculated for different path lengths through the atmosphere using DISORT reveals that *T* is not necessarily linearly proportional to *s* for all *s* for all wavelengths (Figure 7b). This result is expected because multiple regimes are experienced for the range of pressures in the Martian atmosphere and occur over different path lengths depending on the strength of CO_2 absorption at a given wavelength.

4. Artifacts and Residual Atmospheric Spectral Features in CRISM Volcano-Scan Corrected Spectra

The volcano-scan correction does not specifically address potentially large spectral contributions from spatially and temporally variable dust aerosols, ice aerosols, and water vapor that are present in the Martian atmosphere. In addition, the appearance of the 2000 nm bowl-shaped artifact has variable expression depending on options selected in CAT during application of the volcano-scan correction and the temperature dependent wavelength shift of the transmission spectrum relative to the corrected spectrum. We assessed sensitivity to atmospheric

374 dust aerosols, ice aerosols, and water vapor and also present examples showing how the
375 temperature dependent wavelength shift, band depth estimate (BD1 or BD2), and empirical
376 artifact correction options present in CAT further impact the 2000 nm bowl-shaped artifact in
377 CRISM spectra.
378
379 **4.1 Residual Atmospheric Dust Aerosol Features**
380 Dust and ice aerosol abundances are spatially and temporally variable on Mars. Higher
381 dust opacities are typically observed in the Martian perihelion season and there is regional
382 variation in dust loading in the atmosphere [e.g., *Smith et al.*, 2004]. In the NIR, dust aerosols
383 generally impart a negative slope, affect overall spectral brightness, and impact the depth and
384 shape of the CO_2 triplet (Figure 8). Because multiple scattering from dust aerosols brightens
385 dark spectra and darkens bright spectra (Figure 8), with the magnitude of the effect depending on
386 dust opacity, the overall brightness of volcano-scan corrected spectra is not equivalent to surface
387 albedo. This is especially evident in simulated volcano-scan corrected spectra in which the
388 modeled surface spectrum is compared with the volcano-scan corrected spectrum (Figure 5a).
389 The simulated volcano-scan corrected spectrum has a lower albedo and a more negative slope as
390 a result of uncorrected dust aerosol contributions.
391 Variable aerosol contributions between the empirically-derived transmission spectrum
392 and the spectrum to be corrected cause a mismatch in shape between gas bands, which results
393 from aerosol scattering into gas lines. This mismatch in shape between gas bands in the
394 transmission spectrum and the spectrum to be corrected causes additional artifacts near 2000 nm.
395 The effect of dust aerosols on the CO_2 bands is most pronounced in higher opacity images
396 because empirical transmission spectra are derived from images with low dust opacities.

Volcano-scan corrected high opacity spectra exhibit additional 'hash' near 2000 nm because of the larger mismatch in shape between gas bands in the transmission spectrum and the spectrum to be corrected. This is evident in Figure 9 in which volcano-scan corrected CRISM spectra from the same location on Mars but acquired at different times with variable atmospheric conditions are compared. For this comparison, we chose images covering the dusty plains a few km to the south of the Mars Exploration Rover Spirit landing site at Gusev crater. Surface spectra of dusty surfaces are relatively featureless in the NIR, which allows atmospheric residual features to stand out in volcano-scan corrected spectra. Multiple images were acquired of this area at different times of year that capture a variety of atmospheric dust aerosol optical depths. In addition, aerosol optical depth measurements derived from Spirit Pancam observations have been reported [*Lemmon et al.*, 2004]. The 2000 nm bowl-shaped artifact has a variable appearance in example spectra from all three images (Figure 9). Variations are evident that result from different atmospheric conditions and different volcano-scan correction options. All spectra shown in Figure 9 were corrected using transmission spectra with the closest match to the wavelength shift. Both the BD1 and BD2 estimates were used to scale the transmission spectra and the CAT empirical 2000 nm bowl-shaped artifact correction was applied (Figure 9). Volcano-scan corrected spectra from the dustiest image (FRT000553B) exhibit more 'hash' in the 2000 nm artifact (regardless of CAT volcano scan options) that results from changes in gas band shape caused by aerosol scattering.

4.2 Residual Atmospheric Ice Aerosol Features

Water ice aerosols also effect brightness and spectral slope but are particularly problematic because they introduce absorption features at 1500, 2000, and 2400 nm (Figure 10).

The depth of these features depends on the ice aerosol optical depth and grain size (e. g., *Clancy et al*., 2003). Water ice aerosol opacities are highly variable and these aerosols are commonly present at high latitudes during the Martian winter but occur near the equator in the aphelion season [e.g., *Clancy et al.*, 2003].

In order to illustrate the appearance of uncorrected water ice aerosols, we compared volcano-scan corrected spectra from two different locations within the same image. FFC0000A3F6 was acquired over a relatively featureless, dusty area of Mars. The differences between the two spectra shown in Figure 10 result from under corrected water ice aerosols. Absorption features at 1500 and 2000 nm as well as the pronounced negative slope at wavelengths > 2400 nm are evident in the lower spectrum. These water ice aerosol absorptions overlap with some features in hydrated minerals, particularly hydrated sulfates [e.g., *Cloutis et al*., 2006], and can interfere with mineral identifications when present.

4.3 Residual Atmospheric Water Vapor Features

The volcano-scan correction scales all gases (e.g., CO2, H_2O and CO) present in the transmission spectrum by the exponential scaling factor calculated using the ~2010 nm CO_2 band depth estimate. Water vapor concentrations in the Martian atmosphere vary by L_s, latitude, and elevation with typical values between ~ 5 and 20 precipitable μm [e.g., *Smith et al*., 2008]. Under correction of water vapor leaves atmospheric absorption features at ~1400, 1900, and 2600 nm that can impact diagnostic spectral features exhibited by alteration phases that occur near these wavelengths. Figure 11 shows a relatively featureless dusty surface with water absorption features present. Water vapor spectral contributions to surface spectra with alteration phases are less obviously attributable to water vapor because they overlap with mineral

absorption features. This is well illustrated by Figure 12 which shows volcano-scan corrected CRISM spectra from the same carbonate-bearing [*Ehlmann et al.,* 2009] location on Mars but acquired at different times under variable atmospheric conditions. The 2600 nm water vapor feature overlaps with the ~2500 nm carbonate feature and contributes to mismatches between the two different spectra of the same location. In addition, this example shows that the 2000 nm bowl-shaped artifact has a variable appearance and complicates interpretation of the ~1910 nm surface hydration feature. Spectra were corrected using transmission spectra with the closest match to the wavelength shift. Both the BD1 and BD2 estimates were used to scale the transmission spectrum and the CAT empirical 2000 nm bowl-shaped artifact correction was applied (Figure 12a). A ratio spectrum is shown to highlight the fact that apparent differences between spectra taken from the two different images are related to artifacts introduced by the volcano-scan correction as well as residual atmospheric water vapor (Figure 12b). Both FRT00003FB9 and FRT0000A09C have aerosol opacities of ~0.4 calculated using methods described by *Wolff et al*. [2009].

5 Summary and Implications

The empirical 'volcano-scan' correction [*Bibring et al*., 1989; *Langevin et al*., 2005; *McGuire et al.,* 2009] is widely applied to CRISM and OMEGA NIR spectra between ~1000 to ~2600 nm to remove prominent atmospheric CO_2 absorptions with minimal computational investment. However, detailed examination of volcano-scan corrected spectra reveals a bowl-shaped artifact that overlaps with prominent CO_2 features near 2000 nm. The identification and characterization of both artifacts and residual atmospheric features left by the volcano-scan

correction is important for the proper interpretation of CRISM and OMEGA volcano-scan corrected spectra.

Simulation of the volcano-scan correction with radiative transfer modeling enabled assessment of assumptions underlying this empirical method of correction. We found that the most prominent artifact, a bowl-shape centered near 2000 nm, is caused by the inaccurate assumption that absorption coefficients of CO_2 in the Martian atmosphere are independent of column density (Figure 7). This means that transmission is not accurately derived by the division of high and low altitude Martian spectra.

Expression of the 2000 nm artifact varies depending on the choice of the exponential scaling factor used to scale the empirical transmission spectrum during application of the volcano-scan correction (Figure 6). In addition, differences in aerosol scattering into gas bands between the transmission spectrum and the spectrum to be corrected also causes a mismatch in shape between gas bands that results in 'hash' in the 2000 nm region (Figure 9). CAT software version 7.2.1 provides an option to empirically correct the bowl-shape at 2000 nm that largely removes this feature (Figures 9 and 12). However, the performance of this correction on different types of surface spectra acquired under variable atmospheric conditions has not been quantified in the literature and variations between spectra of the same surface acquired under different atmospheric conditions are evident (Figure 12).

Residual atmospheric contributions caused by dust aerosols, ice aerosols, and water vapor are also observed in volcano-scan corrected spectra. Because concentrations of these atmospheric species are temporally and spatially variable, features resulting from these atmospheric contributions in volcano-scan corrected spectra are also variable. Uncorrected dust aerosols modulate the spectral slope and albedo (Figure 8) causing volcano-scan corrected

488 spectra to have inaccurate low frequency shapes (Figure 5a). Uncorrected ice aerosols, when
489 present, result in absorptions centered at 1500 and 2000 nm and a negative slope at 2400 nm
490 (Figure 10). Under corrected water vapor in some volcano-scan corrected spectra results in
491 absorption features centered at 1400, 1870, and 2650 nm (Figure 11). These features are
492 particularly problematic in spectra of alteration minerals (Figure 12).

493 The presence of artifacts and residual atmospheric features left by the volcano-scan
494 correction can impact interpretation of volcano-scan corrected CRISM and OMEGA spectra.
495 Because spurious features introduced by the volcano-scan correction overlap with and obscure
496 diagnostic spectral absorptions that occur between ~1900 and ~2150 nm (e.g., Figure 12),
497 spectral ratios are commonly performed to remove these residual features (as well as calibration
498 artifacts). Comparison of volcano-scan corrected spectra to ratioed volcano-scan corrected
499 spectra highlights artifacts that are evident in unratioed spectra (Figure 12). Spectral ratios of
500 volcano-scan corrected spectra are useful for confirming the presence of narrow absorption
501 features caused by alteration phases. However, although spectral ratios largely remove the
502 volcano-scan artifacts and residual atmospheric contributions, they impact low frequency
503 spectral shape, i.e. continuum shape, and can produce spurious features that mimic spectral
504 absorptions if an inappropriate denominator is utilized. Multiple scattering from atmospheric
505 aerosols is both additive and multiplicative; therefore, aerosol spectral contributions are not
506 completely removed by ratioing. In addition, the amplitude of ratio spectra is arbitrary and
507 cannot be related to physically meaningful units. Quantitative spectral analyses that address
508 band shape, band depth, and mineral abundances are strongly dependent on the quality of
509 atmospherically corrected spectra. Because of the presence of spurious features and/or
510 uncorrected atmospheric contributions in volcano-scan and ratio spectra, radiative transfer

511 modeling is necessary for quantitative analyses [e.g., *Arvidson et al*., 2006; *McGuire* et al.,2008;

512 *Poulet et al*., 2009a; *Poulet et al*., 2009b; *Cull et al*., 2010a; *Cull et al*., 2010b; *Liu et al*., 2012].

513 **REFERENCES**
514
515 Arvidson, R. E., et al. (2006), Nature and origin of the hematite-bearing plains of Terra
516 Meridiani based on analyses of orbital and Mars Exploration rover data sets, J. Geophys.
517 Res., 111, E12S08, doi:10.1029/ 2006JE002728.
518 Bibring, J-P., et al. (1989), Results from the ISM experiment *Nature*, 341, 591-592.
519 Bibring, J.-P., et al. (2004), OMEGA: Observatoire pour la Minéralogie, l'Eau, les Glaces et
520 l'Activité, in *Mars Express: The Scientific Payload*, edited by A. Wilson, Eur. Space
521 Agency Spec. Publ., ESA SP 1240, 37–49.
522 Bibring, J.-P., et al. (2005), Mars surface diversity as revealed by the OMEGA/Mars Express
523 observations, *Science*, 307, 1576–1581, doi:10.1126/science.1108806.
524 Clancy, R.T. et al. (2003), Mars aerosol studies with the MGS TES emission phase function
525 observations: Optical depths, particle sizes, and ice cloud types versus latitude and solar
526 longitude, *J. Geophys. Res*, Research 108(E9): 5089. doi:10.1029/2003JE002058.
527 Cloutis, E. A., et al. (2006), Detection and discrimination of sulfate minerals using reflectance
528 spectroscopy, *Icarus*, 184, 121–157, doi:10.1016/jicarus.2006.04.003.
529 Cull, S., R. E. Arvidson, M. Mellon, S. Wiseman, R. Clark, T. Titus, R. V. Morris, and P.
530 McGuire (2010a), Seasonal H2O and CO2 ice cycles at the Mars Phoenix landing site: 1.
531 Prelanding CRISM and HiRISE observations, *J. Geophys. Res.*, 115,
532 E00D16, doi:10.1029/2009JE003340.
533 Cull, S., R. E. Arvidson, R. V. Morris, M. Wolff, M. T. Mellon, and M. T. Lemmon (2010b),
534 Seasonal ice cycle at the Mars Phoenix landing site: 2. Postlanding CRISM and ground
535 observations, *J. Geophys. Res.*, 115, E00E19, doi:10.1029/2009JE003410.
536 Ehlmann et al. (2009), Identification of hydrated silicate minerals on Mars using MRO-CRISM:
537 Geologic context near Nili Fossae and implications for aqueous alteration, *J. Geophys.*
538 *Res*, 114, E00D08, doi:10.1029/2009JE003339,
539 Langevin, Y., F. Poulet, J.-P. Bibring, B. Gondet (2005), Sulfates in the northern polar region of
540 Mars detected by OMEGA/Mars Express, *Science*, 307, 1584-1586.
541 Lemmon, M. T., et al. (2004), Atmospheric imaging results from the Mars Exploration
542 Rovers: Spirit and opportunity, Science, 306, 1753–1756, doi: 10.1126/science.1104474.
543 Liu, Y., R. E. Arvidson, M. J. Wolff, M. T. Mellon, J. G. Catalano, A. Wang, and J. L. Bishop
544 (2012), Lambert albedo retrieval and analyses over Aram Chaos from OMEGA
545 hyperspectral imaging data, *J. Geophys. Res.*, 117, E00J11,doi:10.1029/2012JE004056.
546 McGuire, P. C. et al., (2009), An improvement to the volcano-scan algorithm for atmospheric
547 correction of CRISM and OMEGA spectral data, *Adv. in Planet. Space Sci.*, *57*,
548 10.1016/j.pss.2009.03.007.
549 Murchie, S., R. E. Arvidson, P. Bendini, K. Beisser, J.-P. Bibring, J. Bishop, J. Boldt, P.
550 Cavender, T. Choo, R. T. Clancy, E. H. Darlington, D. Des Marais, R. Espiritu, D. Fort,
551 R. Green, E. Guinness, J. Hayes, C. Hash, K. Heffernan, J. Hemmler, G. Heyler, D.
552 Humm, J. Hutchenson, N. Izenberg, R. Lee, J. Lees, D. Lohr, E. Malaret, T. Martin, J. A.
553 McGovern, P. McGuire, R. V. Morris, J. F. Mustard, S. Pelkey, E. Rhodes, M. Robinson,
554 T. Roush, E. Schafer, G. Seagrave, F. P. Seelos, IV, S. Slavney, M. Smith, W.-J. Shyong,
555 K. Stohbehn, H. Taylor, P. Thompson, B. Tossman, M. Wirzburger, and M. Wolff

(2007), Compact Reconnaissance Imaging Spectrometer for Mars (CRISM) on Mars Reconnaissance Orbiter (MRO), *J. Geophys. Res*, *112*, E05S03, doi:10.1029/2006JE002682.

Mustard, J., et al. (2008), Hydrated silicate minerals on Mars observed by the CRISM instrument on MRO, *Nature*, 454, 305– 309, doi:10.1038/nature07097.

Poulet, F., et al (2009a), Quantitative compositional analysis of martian mafic regions using the MEx/OMEGA reflectance data 1. Methodology, uncertainties and examples of application, *Icarus*, 201, 69-83, doi:10.1016/j.icarus.2008.12.025.

Poulet, F., et al (2009b), Quantitative compositional analysis of martian mafic regions using the MEx/OMEGA reflectance data 2. Petrological implications, *Icarus*, 201, 84-101, doi:10.1016/j.icarus.2008.12.042.

Rothman, L.S. et al. (2009), The HITRAN 2008 molecular spectroscopic database, *J. of Quant. Spect. Rad. Transfer*,110, 533-572.

Smith, M.D. (2004), Interannual Variability in TES Atmospheric Observations of Mars During 1999-2003. Icarus, 167, 148-165.

Smith, M. D. (2008), Spacecraft Observations of the Martian Atmosphere, Annual Review of Earth and Planetary Sciences, 36, 191–219, doi:10.1146/annurev.earth.36.031207.124334.

Smith, M. D., M. J. Wolff, R. T. Clancy, and S. L. Murchie (2009), Compact Reconnaissance Imaging Spectrometer observations of water vapor and carbon monoxide, *J. Geophys. Res*, 114, E00D03, doi:10.1029/2008JE003288.

Stamnes, K., S. Tsay, W. Wiscombe, and K. Jayaweera (1988), Numerically stable algorithm for discrete-ordinate-method radiative transfer in multiple scattering and emitting layered media, *Appl. Opt.*, *27*, 2502-2509.

Stamnes, K., S.-C. Tsay, I. Laszlo (1999), DISORT , a general purpose Fortran program for discrete-ordinate-method radiative transfer in scattering and emitting layered media: Documentation and methodology, pp 112.

Thomas, G. E., Stamnes, K. (2002), *Radiative transfer in the atmosphere and ocean*, Cambridge University Press, New York, 546pp.

Wolff, M. J., M. D. Smith, R. T. Clancy, R. E. Arvidson, M. Kahre, F. P. Seelos IV, S. Murchie, and H. Savijarvi (2009), Wavelength dependence of dust aerosol single scattering albedo as observed by the Compact Reconnaissance Imaging Spectrometer, *J. Geophys. Res.*, 114, E00D04, doi:10.1029/2009JE003350.

FIGURES

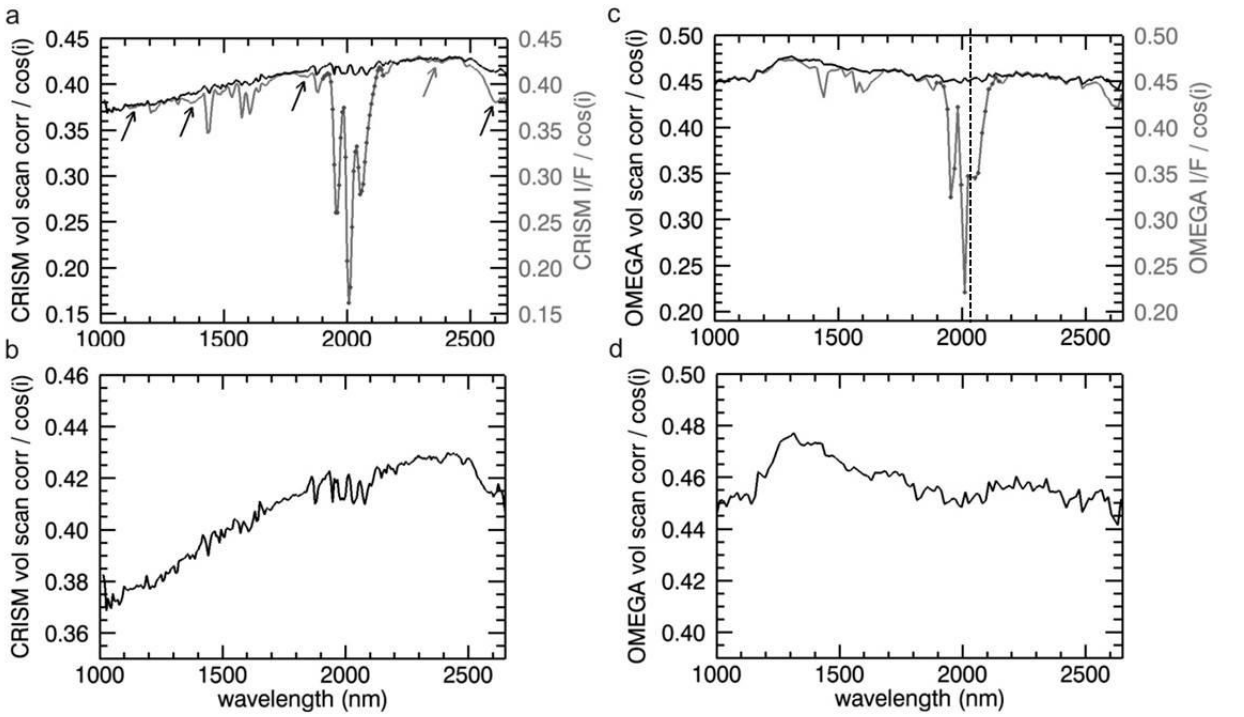

Figure 1. a) CRISM spectrum extracted from FFC000061C4 before (gray) and after (black) volcano-scan correction. Because the transmission spectrum and corrected spectrum were both derived from the same image, the temperature dependent wavelength shift is minimized. Gray dots show CRISM channel positions located between 1900 and 2150 nm (7 nm intervals). Black arrows indicate atmospheric H_2O vapor absorptions centered near 1130, 1380, 1880, and 2590 nm. A shallow CO feature near 2350 nm is also present. Unlabeled absorptions result from atmospheric CO_2. b) Close up of the black CRISM spectrum shown in part (a). Note the bowl-shape and 'hash' in the 2000 nm region. c) OMEGA spectrum extracted from ORB0037_2 before (gray) and after (black) volcano-scan correction. Gray dots indicate OMEGA channel positions located between 1900 and 2150 nm. OMEGA acquires data at 14 nm intervals; however the channel at 2040 nm (dotted line) is dead. Lack of data at this wavelength causes the longest wavelength minimum in the CO_2 triplet to appear less well defined in OMEGA spectra than CRISM spectra. d) Close up of the black OMEGA spectrum shown in part (c). Both CRISM and OMEGA spectra were extracted from dust covered surfaces located to the south of Olympus Mons. Differences between the CRISM and OMEGA spectra shown in parts (b) and (d) could result from calibration characteristics as well as differences in viewing geometries and atmospheric conditions.

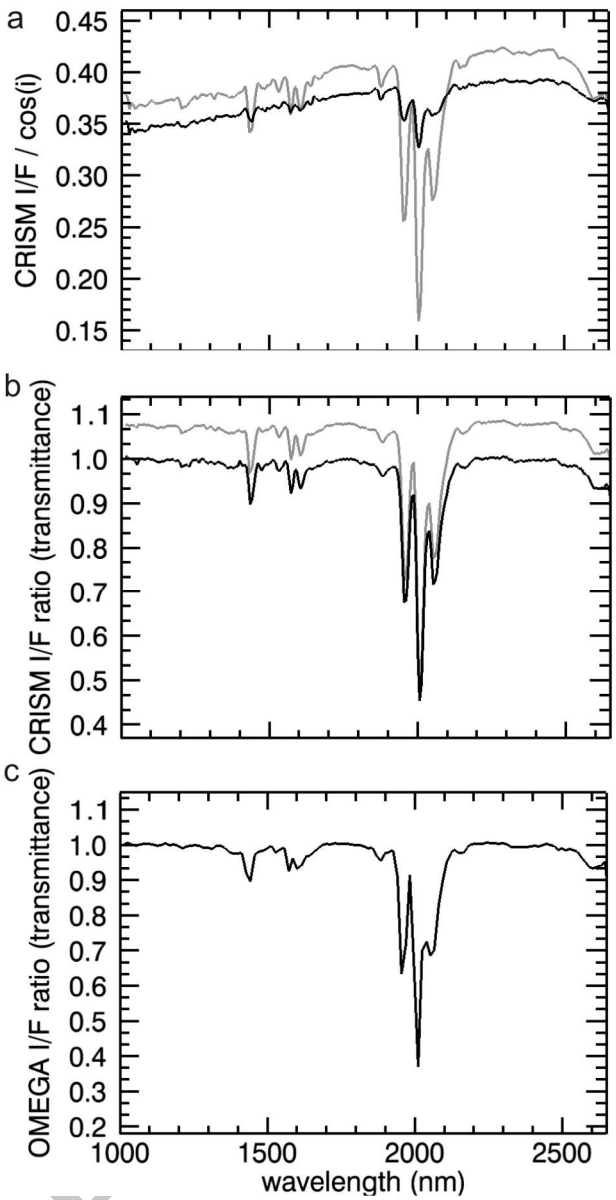

Figure 2. a) CRISM high (black) and low (gray) altitude spectra acquired at the base and summit of Olympus Mons, respectively, extracted from FFC000061C4. b) CRISM scaled (black) and unscaled (gray) transmission spectra generated from low and high altitude spectra shown in part (a). c) OMEGA scaled transmission spectrum.

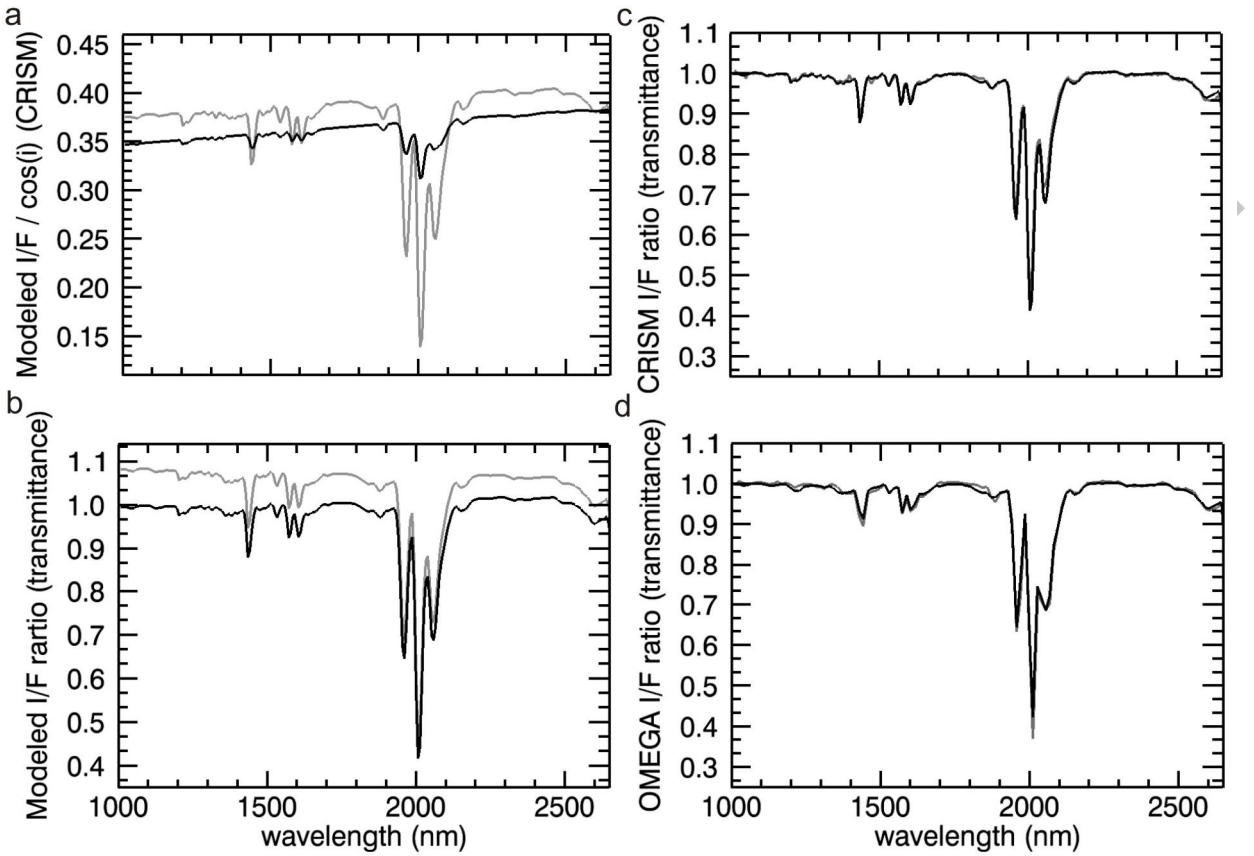

Figure 3. a) DISORT modeled high (black) and low (gray) altitude spectra convolved to CRISM spectral resolution computed using pressure/temperature profiles appropriate for the base and summit of Olympus Mons, respectively. A dust opacity of 0.3 and 5 precipitable μm of water vapor were modeled for the low altitude spectrum and no dust or water vapor were modeled for the high altitude spectrum. b) Scaled (black) and unscaled (gray) transmission spectra generated from spectra shown in part (a). c) Modeled transmission spectrum (black) overlain on an actual CRISM transmission spectrum (gray). d) Modeled transmission spectrum (black) overlain on an actual OMEGA transmission spectrum (gray).

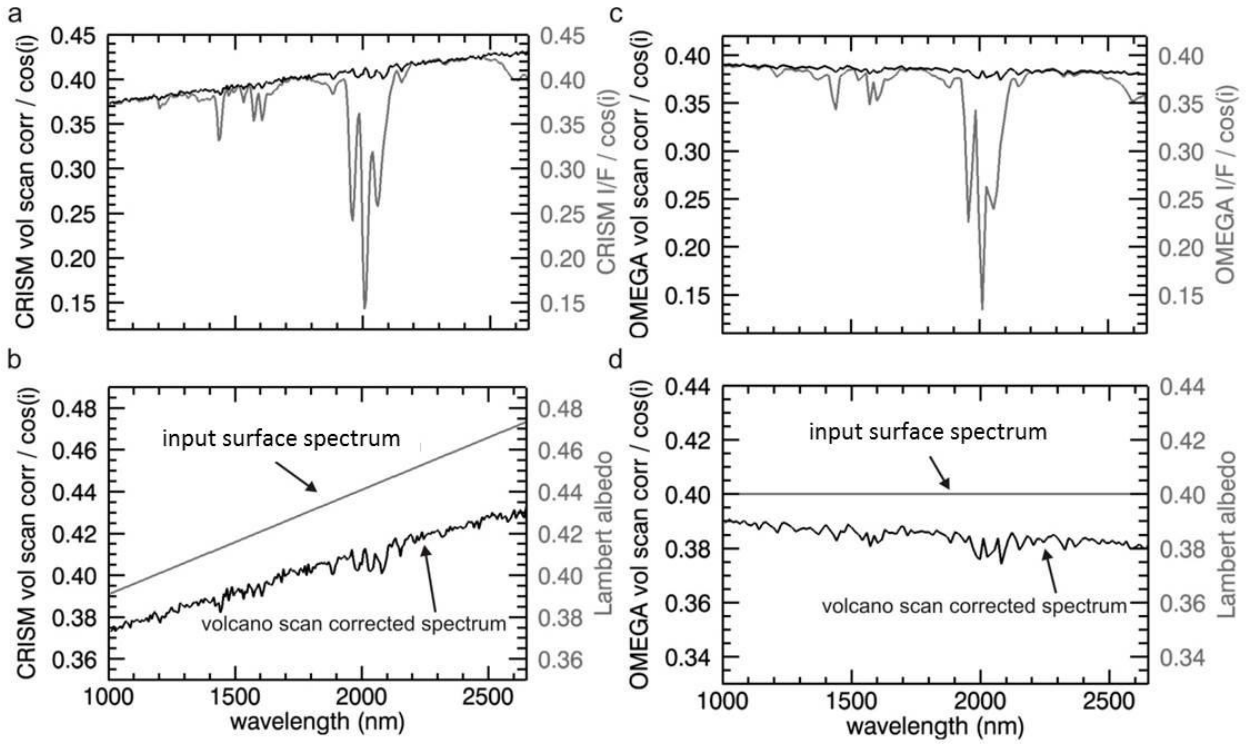

Figure 4. a) Modeled CRISM spectrum before (gray) and after (black) simulated volcano-scan correction. b) Close up of the black spectrum shown in part (a) but with the input surface spectrum over-plotted in gray. A linear function was used to model the surface specrum to highilight artifacts in the volcano-scan correction. Perfect atmospheric correction would result in the black and gray spectra overlapping. c-d) Same as parts (a-b) but for OMEGA spectral resolution. Although CRISM and OMEGA spectra shown in parts (a) and (c) were both acquired at Olympus Mons, the CRISM spectrum has a positive slope whereas the OMEGA spectrum is near horizontal. This mismatch in continuum shape between the two datasets, as released in the PDS, is likely related to specifics of the instrument calibrations and is beyond the scope of this paper to address.

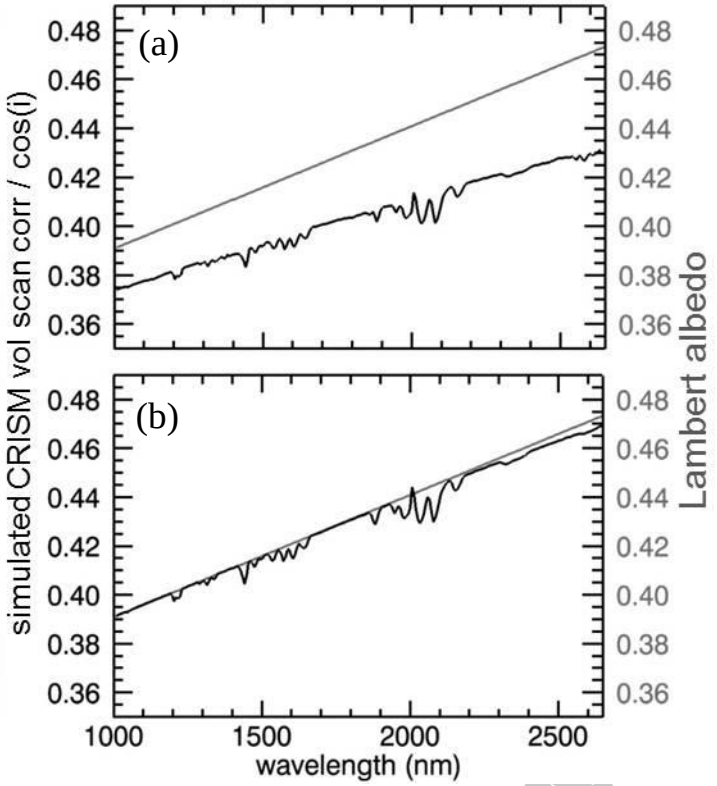

630 Figure 5. (a) Simulated CRISM volcano-scan corrected spectrum (black) and input surface
631 Lambert albedo spectrum (gray). Aerosols were present in both the simulated transmission
632 spectrum (Figure 3b, black) and the modeled spectrum that was corrected. Noise was not added
633 to the simulation to highlight artifacts. Perfect atmospheric correction would result in the black
634 spectrum overlapping with the gray spectrum. (b) Same as part (a), but with no aerosols
635 modeled in either the simulated transmission sepctrum or the corrected spectrum. Perfect
636 atmospheric correction would result in the black spectrum overlapping with the gray spectrum.

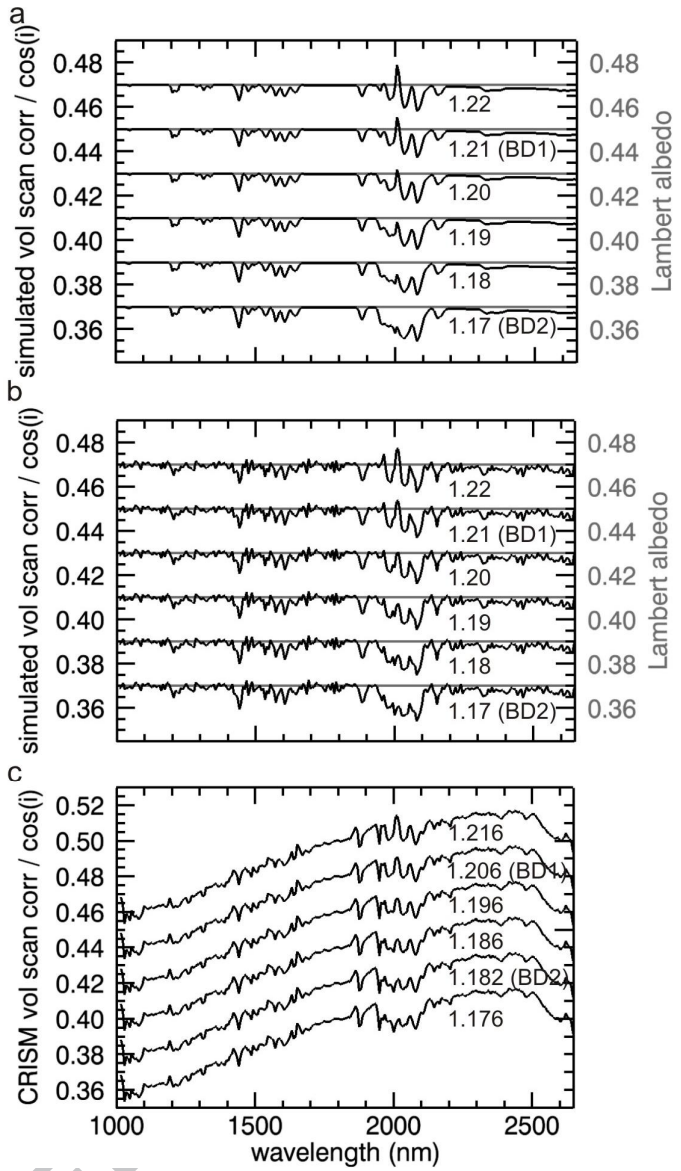

Figure 6. a) Black lines: Simulated volcano-scan corrected spectra using simulations with no aerosols modeled, offset for clarity. The exponential scaling factors (see Equation 8) used to create the simulated volcano-scan corrected spectra were systematically varied. The exponential scaling factor used to scale the simulated transmission spectrum prior to division (labeled on plot) was the only variable changed among the plotted spectra. Note the change in character of the artifacts near 2000 nm as the scaling factor value is increased. The gray lines show actual surface spectra (perfect atmospheric correction would result in the black spectra overlapping with the gray spectra). b) Same as part (a) but with noise added. c) Actual CRISM volcano-scan corrected spectra with systematically varied exponential scaling factors, offset for clarity. The exponential scaling factor used to scale the transmission spectrum prior to division (labeled on plot) was the only variable changed among the plotted spectra. Note the change in character of the artifacts near 2000 nm as the scaling factor value is increased.

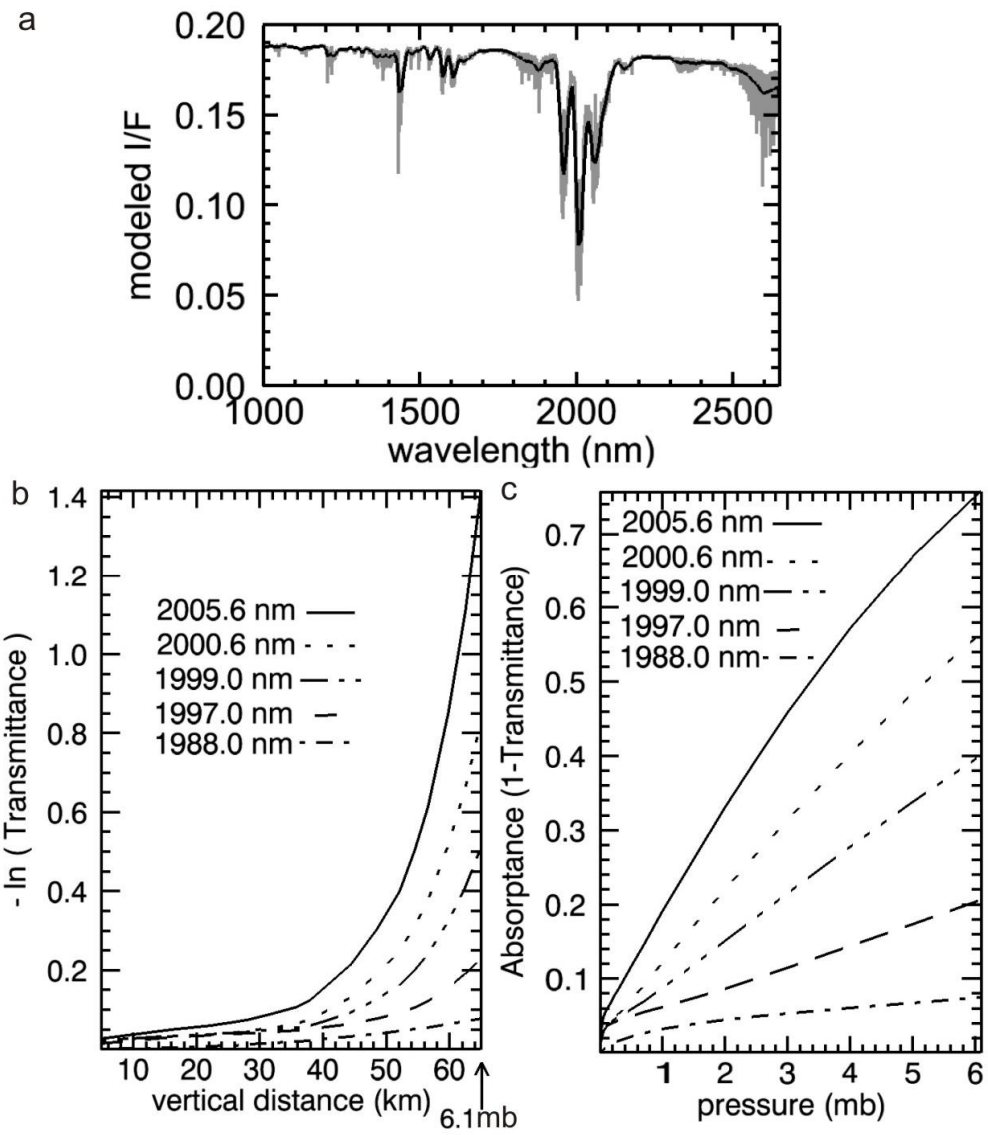

649 Figure 7. a) Shapes of gas absorption features measured by CRISM are a convolution of very
650 narrow gas bands and the CRISM instrument response function. Gray line: DISORT generated
651 I/F spectrum with I/F values calculated every 0.4 nm. Black line: High spectral resolution gray
652 spectrum convolved to CRISM spectral resolution. b) Plots of negative natural logarithm
653 transmittance calculated using DISORT versus vertical distance at several different wavelengths.
654 Vertical distance times 2 is equivalent to the total path length, *s*. According to equation 3, there
655 should be a linear relationship between the negative natural logarithm of transmittance and
656 distance, *s*. If this were the case, then the curves would be linear with slopes of *k*. For this plot,
657 the top of the atmosphere (vertical distance of 0) was set to 65 km above the surface, a distance
658 at which atmospheric pressure is negligible. At the surface (vertical distance of 65 km), the
659 pressure is 6.1 mb, which is Mar's average atmospheric pressure. c) Plots of absorptance versus
660 pressure. Pressure is exponentially proportional to vertical distance (assuming constant
661 temperature). Therefore, according to equation 3, these curves should also appear linear.

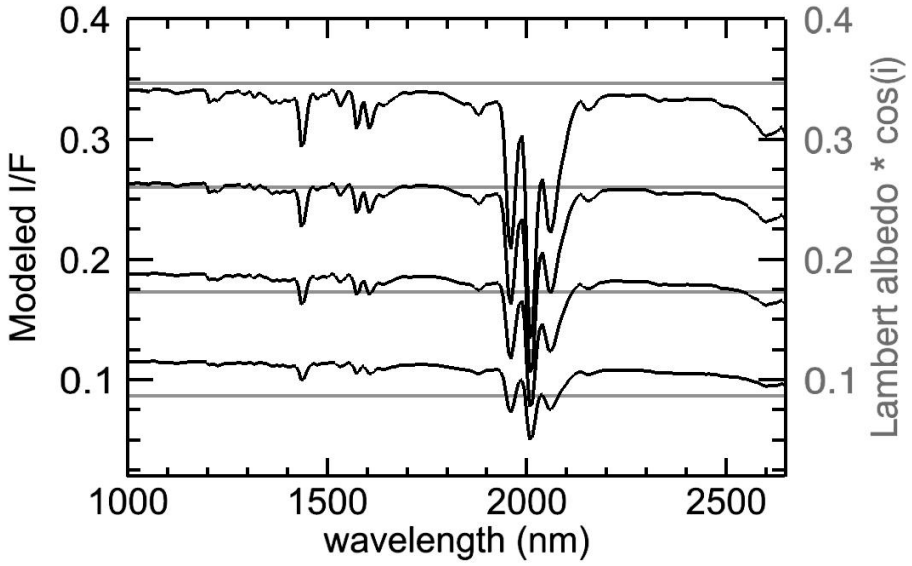

Figure 8. DISORT generated I/F spectra (black lines) for surface Lambert albedo spectra shown by gray lines. Long wavelength I/F spectral shape is affected by atmospheric dust, which imparts a negative slope. The surface Lambert albedo spectra with no atmospheric contributions (gray lines) have slopes of 0. Multiple scattering caused by dust aerosol particles brightens I/F spectra of dark surfaces and darkens spectra of bright surfaces. I/F spectra were modeled with DISORT for a modest dust opacity of 0.6 at 900 nm and a viewing geometry of i = g = 30°, e = 0° and surface Lambert albedos of 0.1, 0.2, 0.3, or 0.4 at all wavelengths.

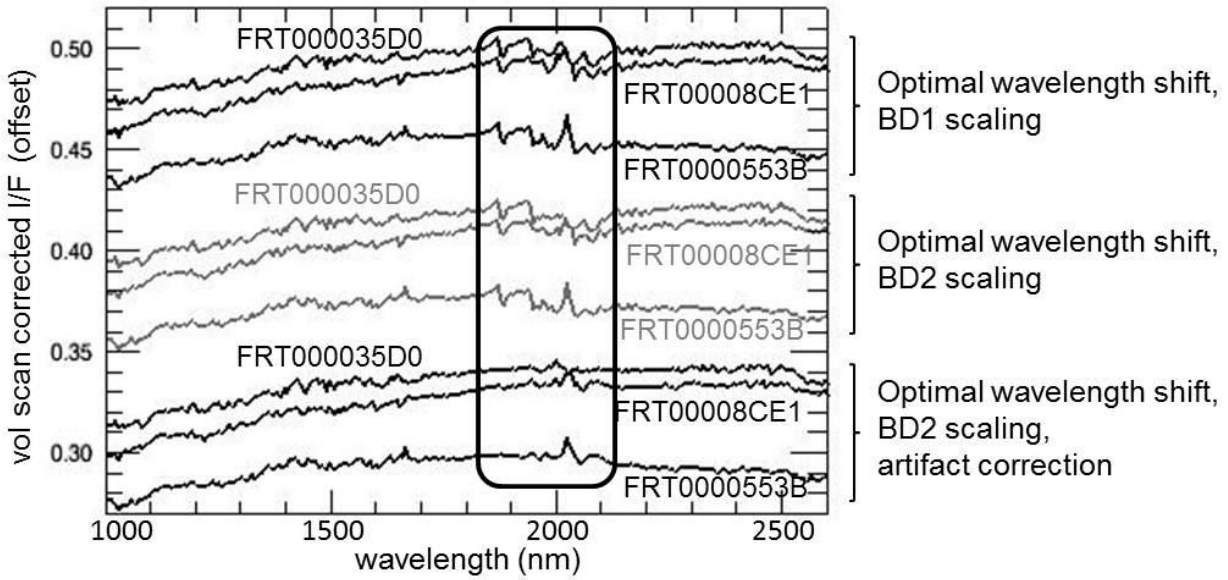

669 Figure 9. CRISM volcano-scan corrected spectra from the same location (-14.656N, 175.463E)
670 in Gusev crater images FRT000035D0 (τ = 0.4), FRT0000553B (τ = 0.6), and FRT00008CE1 (τ
671 = 0.9) (10x10 pixel average). FRT0000553B has the highest dust opacity and the most hash in
672 the 2000 nm bowl-shaped artifact. The 2000 nm bowl-shaped artifact has a different appearance
673 depending on the transmission spectrum and exponential scaling factor applied during the
674 volcano-scan correction.

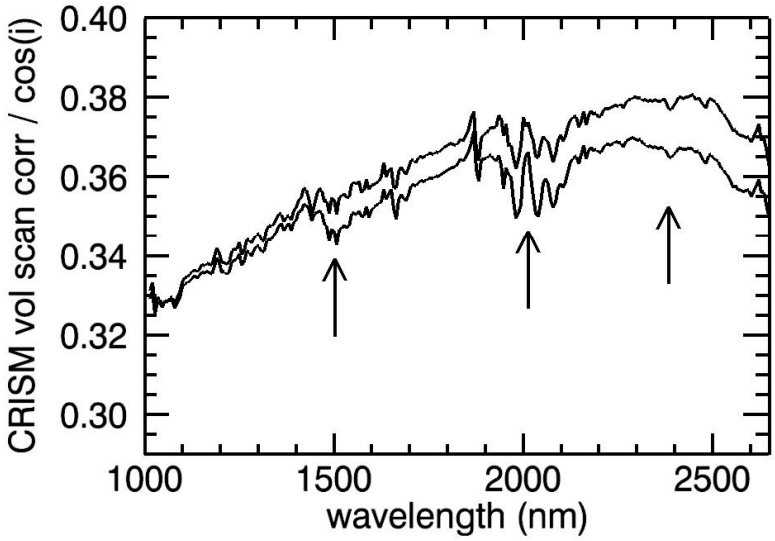

675 Figure 10. Volcano-scan corrected CRISM I/F spectra extracted from FFC0000A3F6. The
676 lower spectrum has distinct water ice aerosol features, which include absorptions centered at
677 1500 and 2000 nm and a decrease in slope starting at 2300 nm. The 2000 nm ice absorption is
678 partially obscured by artifacts induced by the volcano-scan correction.

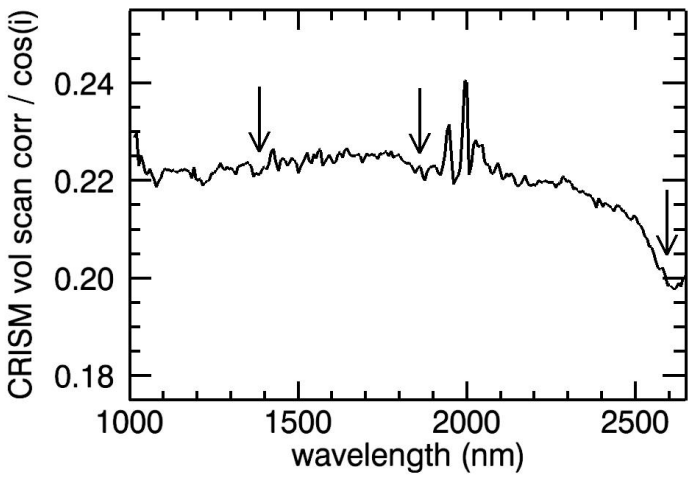

679 Figure 11. Volcano-scan corrected CRISM I/F spectrum extracted from FRT0000CAB3 in which
680 water vapor is under-corrected. The water vapor absorption features near 1380, 1880, and 2590
681 nm are indicated with black arrows. Note, the CO_2 triplet near 2000 nm is poorly corrected as a
682 result of high atmospheric dust opacity (> 1.0) at the time of image acquisition.

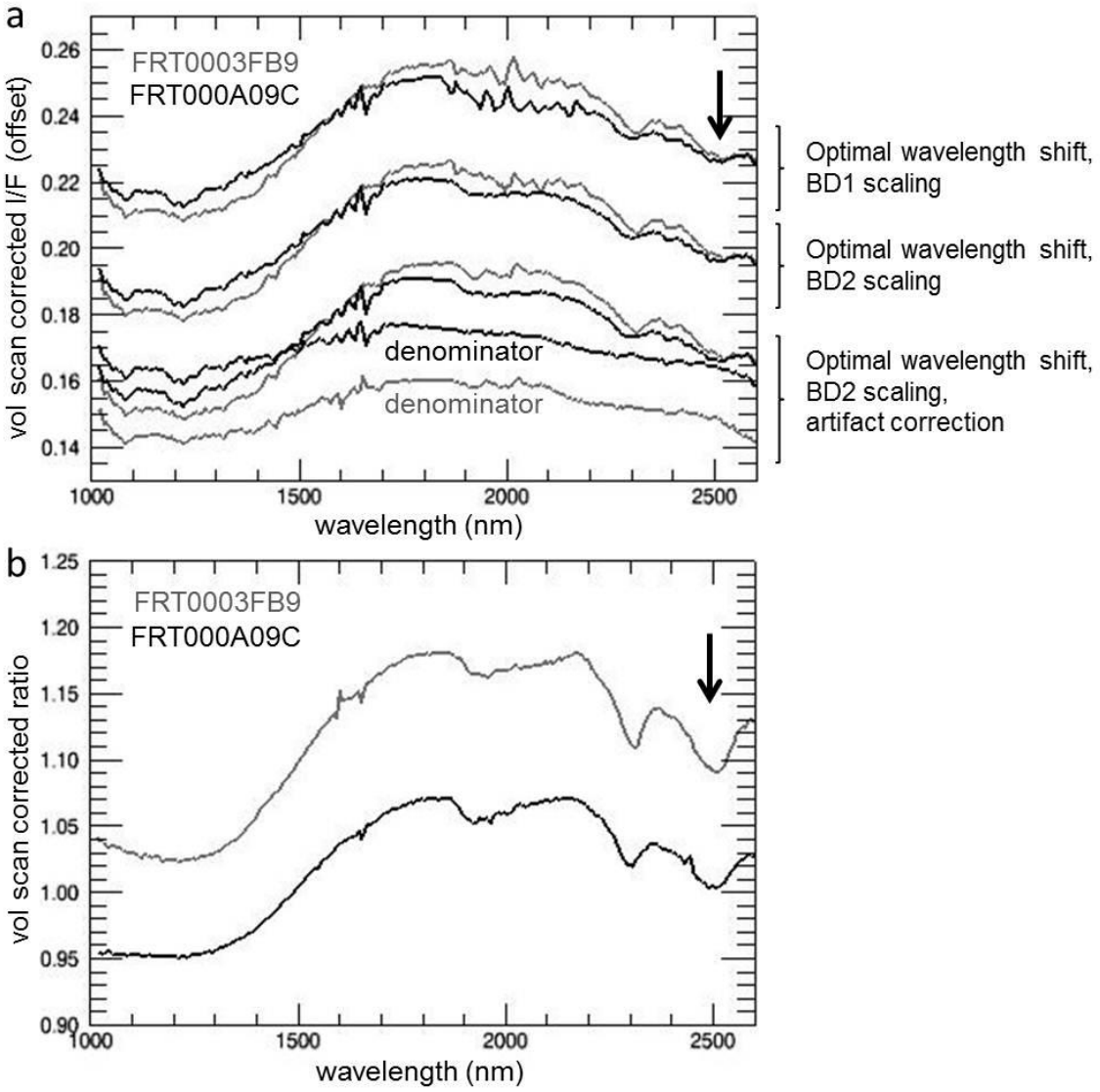

683 Figure 12. (a) CRISM volcano-scan corrected spectra from the same location (21.24N, 78.6E)
684 covering a carbonate- and phyllosilicate- bearing outcrop (10x10 pixel average) in Nili Fossae.
685 Spectra from FRT00003FB9 were extracted from column 220, line 21 and spectra from
686 FRT0000A09C from column 52, line 100. Although spectra were extracted from roughly the
687 same location, they are not expected to have identical brightnesses because of differences in
688 illumination resulting from different solar incidence angles and measurement emission angles.
689 The 2000 nm bowl-shaped artifact, which overlaps with a ~1910 nm surface hydration feature,
690 has a different appearance depending on the transmission spectrum and exponential scaling
691 factor applied during volcano-scan correction. Variable amounts of residual water vapor alter
692 the expression of the 2500 nm carbonate feature (black arrow). This feature looks more similar
693 in ratio spectra shown in part (b). (b) Spectral ratios calculated using the lower set of spectra
694 (optimal wavelength shift, BD2 scaling, artifact correction) shown in in part (a). Denominator
695 spectra used to generate these ratio spectra were extracted from the same columns as the

corresponding numerator spectra rather than the same surface location to minimize column dependent artifacts. Note, it was not possible to extract spectra from both the same surface location and corresponding columns as numerator spectra due to CRISM measurement geometry. Ratio spectra remove volcano-scan correction artifacts and highlight narrow absorption features. However, low frequency spectral shape is variable between numerator spectra shown in part (a) and ratioed spectra shown in part (b). In addition, the artifact correction as currently implemented in CAT v7.2.1 impacts wavelengths between ~1760 and 2240 nm and contributed to the apparent peak at ~ 2200 nm in the gray ratioed spectrum.

The empirical volcano scan correction leaves a prominent artifact near 2000nm.

Spectral albedo and slope are modified by uncorrected atmospheric aerosols.

Residual water vapor features overlap with mineral hydration features.